Effect of the elevated temperature on the wear behavior of Laser Metal Deposition IN718 repairs

Théo Zurcher, Gaëtan Bouvard, Jean-Christophe Abry, Vincent Fridrici, Éric Charkaluk

Effect of the elevated temperature on the wear behavior of Laser Metal Deposition IN718 repairs

Théo Zurcher[1,2,*], Gaëtan Bouvard[1], Jean-Christophe Abry[1], Vincent Fridrici[1,**], Éric Charkaluk[2,***]

[1]Ecole Centrale de Lyon, Laboratoire de Tribologie et Dynamique des Systèmes, UMR CNRS 5513 ECL-ENTPE, Ecully, 69130, France
[2]Ecole Polytechnique, Laboratoire de Mécanique des Solides, UMR CNRS 7649, Palaiseau, 91120, France
*theo.zurcher@polytechnique.edu
**vincent.fridrici@ec-lyon.fr
***eric.charkaluk@polytechnique.edu

Abstract

IN718, a nickel-based superalloy popular in aerospace, has good high-temperature mechanics/corrosion resistance. Laser Metal Deposition (LMD) repairs using IN718 are extensively explored, yet few studies delve into their tribological aspects. This research examines post-treated IN718 coatings, mimicking rapid repairs, investigating their high-temperature tribological behavior. Samples underwent tribological tests at diverse loads and temperatures. Results show the scanning strategy does not impact the wear behavior. At elevated temperatures, a glaze layer forms in the contact zone, impacting lubrication and surface protection based on its uniformity. Despite its advantageous lubricating ability, at 400°C and 50 N force, the oxidized debris layer lacks mechanical stability. IN718 LMD repairs manifest enhanced high-temperature wear resistance compared to ambient conditions, attributed to the glaze layer.

Keywords: Additive manufacturing, Wear, Nickel-based alloy, High temperature

1. Introduction

Unlike conventional repair methods, the Laser Metal Deposition (LMD) process has the advantage of achieving high-resolution repairs on complexly shaped metal parts with a minimal thermally affected zone [1], [2]. The process is widely used, particularly for repairing components in the aerospace /aeronautics sector. In fact, this method is employed, among other things, to repair aircraft engines turbine blades [3]–[5]. These parts undergo significant wear and require maintenance operations as they operate in severe environments with high mechanical stresses and temperatures. In such conditions, these parts can either be replaced or repaired. Taking the example of an aircraft engine turbine blade, it has been estimated that repairing 10% of its volume reduces its carbon footprint by 45% compared to replacing it with a new one [4]. Therefore, for both economic and environmental reasons, companies are increasingly turning to this additive manufacturing process to repair complex metallic parts.

The extreme conditions in which some parts operate require alloys with good mechanical properties and resistance to corrosion at high temperatures. This is the case of nickel-based superalloys like IN718 thank to the precipitation of strengthening phases (γ' and γ''). This alloy is the subject of extensive research in additive manufacturing because, unlike some other grades in the same family, it exhibits also very good weldability, making it easier to optimize process parameters for shaping [6].

The wear behavior of IN718 repaired by LMD has not been extensively studied in the literature and in the case of sliding wear, most of the studies have been conducted at room temperature. In a previous author's work, it has been shown that, at room temperature, the scanning strategy and the sliding direction according to the bead orientation do not impact the wear behavior of the IN718 LMD repairs [7]. As the number of cycles increases, the wear volume tends to stabilize because of the appearance of an oxidized layer that protects the repairs and wears the metallic counter body. Finally, the competitiveness of the wear resistance of the IN718 LMD repairs compared to a conventionally manufactured IN718 part has been highlighted.

Recently, Lui et al. showed also the importance of heat treatments on the wear resistance of this alloy deposited by LMD [8] and they observed an anisotropic behavior of wear properties depending on the tribologically loaded surfaces. The detrimental impact of Laves phases has also been highlighted [7], [8]. Still at room temperature, Xu et al. showed that, by optimizing process parameters, it was possible to improve the wear resistance of as-built LMD parts [9]. Onuike et al. also studied the wear resistance of restored parts using different manufacturing strategies [10]. Song et al. investigated IN718 deposited by LMD with the addition of graphene to enhance wear resistance [11]. By adding TiC particles, Hong et al. observed that the wear properties are greatly improved when the laser energy input is high enough [12].

At high temperatures, Liu et al. recently studied the tribological behavior of IN718 deposited by LMD and subsequently laser polished. They showed that, after being polished, the IN718 had better wear properties [13]. Lu et al. studied the wear properties of IN718 deposited on a Ti-6Al-4V substrate with a transition composition route [14]. They observed at high temperature that the chromium and vanadium, added for the transition route, allow the appearance in the contact of oxides in the glaze layer that improve the wear resistance of the IN718. Samuel et al. studied the wear resistance of this superalloy shaped by LPBF (Laser Powder Bed Fusion) up to 600°C [15]. Unlike Lu et al., they demonstrated that as the test temperature increases, wear resistance properties decrease because of the appearance of an unlubricated NiO layer and severe delamination. A few articles have also studied the fretting wear behavior of this alloy deposited by LMD at both room temperature and high temperature [16], [17].

Therefore, based on the brief previously presented literature review, it can be concluded that the study of high-temperature wear resistance of IN718 parts repaired by LMD is a rarely explored subject and still not well understood.

In this way, this paper focuses on the wear behavior of parts repaired by LMD with IN718 at high temperatures. Samples are repaired using different scanning strategies and are subjected to flat-on-flat reciprocating linear wear tests. Tests were conducted at different temperatures and loads in this study. The evolution of the coefficient of friction (COF) as well as the wear volume were analyzed. Subsequently, in order to understand the tribological phenomena, the two contacting bodies were observed after test through various characterization methods. Effect of temperature on the wear properties of IN718 obtained by LMD is analyzed through the changes in wear mechanisms, induced by the interactions between the rubbing surfaces and the environment.

2. Materials & Methods

2.1. Samples manufacturing

The samples were produced using a BeAM LMD machine (*mobile* model) equipped with a YLR fiber laser with a wavelength of 1070 nm and a maximum power of 500 W. The powder is conveyed underneath the laser's focal point using an argon gas flow. Process parameters are provided in **Table 1**. and were chosen in order to manufacture samples with high density. Powder flow is controlled by a bowl system mounted on a rotating platform. The IN718 powder was supplied by Oerlikon, and its chemical composition is summarized in **Table 2**. Repairs measuring 55 x 55 x 2 mm^3 are made on an 85 x 65 x 12 mm^3 substrate made of low-alloy steel (XC48). The repaired surfaces are milled to reduce surface roughness. The samples were milled using an 80 mm diameter reamer with 7 carbide flutes, at a rotation speed of 95 rpm, a table feed of 29 mm/min, and a depth of cut of 0.2 mm. After machining, the height of the repairs is 1.5 mm. The final average arithmetic surface roughness (Sa) of the sample surfaces is 0.7 µm. The choice of material meets industrial requirements. However, it is worth noting that, due to the significant repair height, the choice of substrate material does not impact the results. To imitate a fast repair, no further post-treatments were applied to those samples (such as heat-treatments, Hot Isostatic Pressing (HIP), etc.).

To conduct high-temperature tests, two holes with a diameter of 6.5 mm each were drilled into the substrate to accommodate 150 W heating cartridges with a 6 mm diameter. Another small hole of 1.1 mm diameter was drilled in between the two holes to insert a small thermocouple of 1 mm diameter at the core of the samples to monitor the temperature. The sample geometries are presented in **Figure 1**a.

Table 1. Process parameters used

Parameters	Power (W)	Scanning speed (mm/min)	Powder flow rate (g/min)	Overlap (%)	Vertical increment (mm)	Working distance (mm)
Value	325	2250	7	30	0.2	3.5

Table 2. Chemical composition of the powder

Elements	Ni	Cr	Fe	Nb	Mo	Ti	Al	Mn	Co	C	N	Si
IN718 powder (wt%)	Ba.	18.92	18.25	5.15	3.11	0.92	0.42	0.1	0.05	0.05	0.03	0.03

For this study, two manufacturing strategies are examined: the 0° strategy and the 90° strategy. The 0° strategy involves depositing the material with a back-and-forth laser motion without any rotation of the scanning direction between two consecutive layers. The nozzle always returns to the same starting point when depositing a new layer. For the 90° strategy, the laser also follows a back-and-forth motion, but for each new layer, the deposition direction rotates by 90°. Thus, the starting point of the nozzle remains the same every four layers. These two strategies are summarized in **Figure 1**b. Both samples have a density around 99.91 ± 0.04% [18].

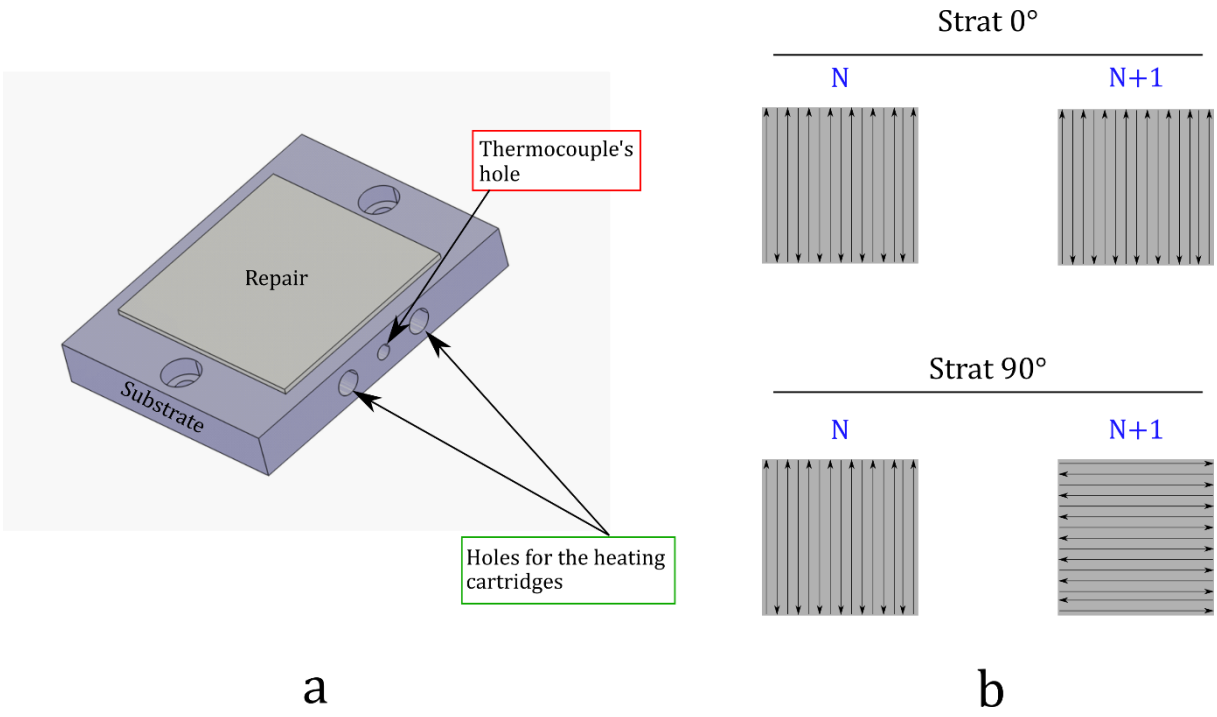

Figure 1. a) 3D computer-aided design drawing of a sample; b) The two studied scanning strategies.

2.2. Tribological tests

Tribological tests were conducted on a homemade linear reciprocating motion test bench. The latter is depicted in **Figure 2**. The latter is the same bench used for the study of the wear resistance of the IN718 LMD repairs at room temperature with the addition of a heating system [7]. It includes a fixed arm that carries the tangential force sensor and the counterbody. In order to approach a conventional wear scenario between two metals, a pin made of 100Cr6 steel with a hardness of 800 HV was used as a counterbody (please note that no particular tribological standards were followed). The loading is applied by adding weights above it. The reciprocating linear motion is driven by an oscillating plate to which the LMD sample is fixed. To protect the test bench from high test temperatures, several features have been added. Firstly, a water box and a layer of thermal insulation act as a buffer between the sample and the oscillating plate. The water inside the water

box is continuously cooled by a water-cooling system. Additionally, a sheet made of stainless steel is attached to the fixed arm to serve as a thermal shield, and a small fan is attached to the arm to remove hot air between the thermal shield and the arm. With such a tribometer, given that the major measurement error comes from the tangential sensor measurement resolution, we estimate the percentage of error of the COF at 1%. It is worth noting that, to limit the COF measurement, the calculation of the COF is performed without using the measured point in the turnarounds.

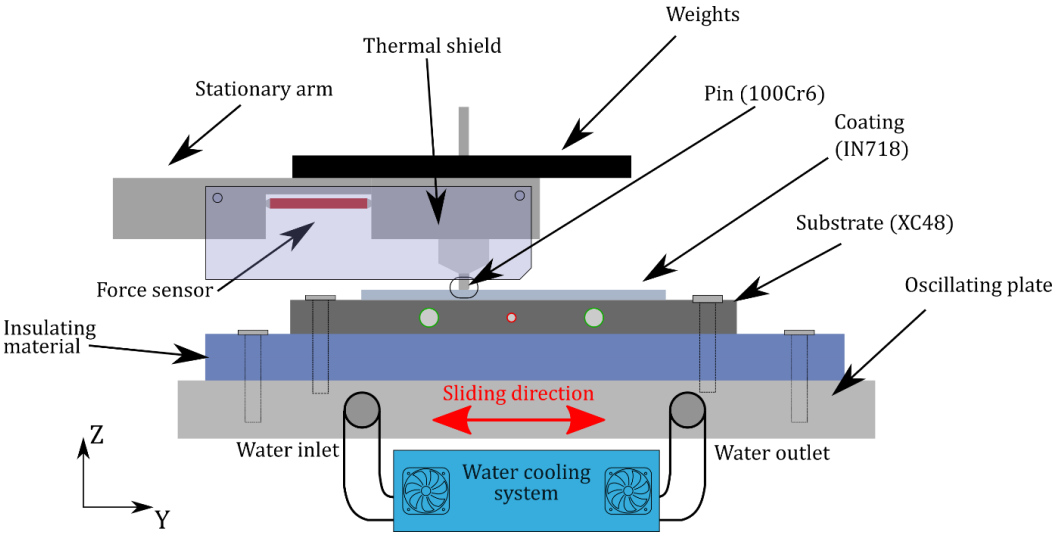

Figure 2. Diagram of the tribological reciprocating test bench.

Before each tribological test, to ensure a conformal contact between the pin and the plane, an in-situ polishing of the pin is performed at room temperature by placing a 400P SiC polishing paper between the two bodies. This polishing is carried out at a frequency of 1 Hz for 2 minutes with a load of 20 N at room temperature. Then, before launching the tribological tests, the heating system is turned on at the setpoint temperature for 30 minutes to ensure that the surface temperature is homogeneous and steady.

All tribological tests were conducted under dry conditions with a frequency of 3 Hz, a stroke length of ±10 mm, for 5,000 cycles, with loads of 20 and 50 N (resulting in an initial average pressure of 6.36 MPa and 15.92 MPa, respectively). The tests were conducted at room temperature, 400°C, and 600°C. For repeatability reasons, all the tribological conditions were tested at least 3 times (except for tests at 50 N tested 2 times for each tribological condition).

During the tribological test, the tangential force F_t is recorded according to the position, for each cycle. From those data, the coefficient of friction (COF) and the total dissipated energy E_d are calculated. The total dissipated energy for N cycles is calculated as follows.

$$E_d = \sum_{i=1}^{N} E_{d,i} = \sum_{i=1}^{N} \int_{-\delta^*}^{+\delta^*} F_t(\delta) d\delta \quad (1)$$

With δ* the stroke length and δ the position.

2.3. Wear characterization

Wear volume was measured using interferometry with a Bruker GT-K1 interferometer. After cleaning the wear track with ethanol-soaked paper, the entire track was scanned using a "stitching" method. To achieve good depth resolution, green light was used. The pin was weighted before and after the

wear test to quantify its wear mass. To determine wear mechanisms, wear tracks on the plane and the contact surface of the pin were observed using a Tescan MIRA FEG Scanning Electron Microscope (SEM). SEM analyses were also complemented with EDX (Energy-Dispersive X-ray) analyses using an Oxford detector. The SEM pictures and EDX maps were acquired with a 10 keV electron beam, with a working distance of 15 mm. The calculation of the oxygen element coverage rate was performed through image analysis using ImageJ software [19]. The EDX maps of the oxygen element were first converted to 8 bits and then binarized to distinguish oxygen from the other elements.

2.4. Material characterization

The top microstructure of the samples has already been studied in detail in previous works [18]. However, for a proper interpretation of the results, some key characteristics are provided here. The top microstructure is highly heterogeneous, with the alternation of small equiaxed grains and large columnar grains, which can lead to hardness heterogeneities. On average, considering both grain families based on their surface percentage, the grain size is 24 µm and 17 µm for Strat 0° and Strat 90°, respectively. Both have a low texture (MUD < 2) and an average core hardness of 300 ± 10 HV.

3. Results & Discussion

3.1. Impact of the scanning strategy

In the literature, it has been shown that the scanning strategy can have an impact on wear performance [10]. Therefore, to confirm this observation at high temperature, tribological tests were conducted at different temperatures with a 20 N load for both studied strategies. **Figure 3** summarizes the results in terms of COF and wear volume as a function of these parameters. Firstly, **Figure 3**a shows that the average COF gradually decreases as the test temperature increases. Moreover, this figure highlights that the choice of repair strategy does not impact the COF. Regarding the evolution of wear volume with temperature shown in **Figure 3**b, it is observed that wear volume decreases with temperature. Similarly to the COF, the laser scanning strategy has no significant impact on wear volume.

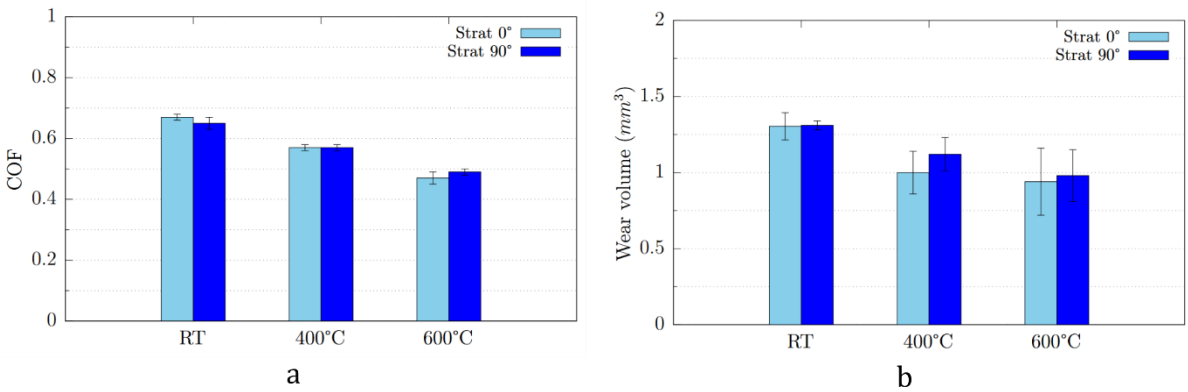

Figure 3. Evolution of the a) COF and the b) wear volume as a function of the temperature and the scanning strategy.

This result is in contradiction with the literature [10]. However, this has already been explained in a previous publication dedicated to room temperature tests [7]. In fact, the lack of influence of the repair strategy on their wear volume is mainly due to the surface nature of the contact (flat-on-flat, large contact area, compared to the size of microstructural characteristics), which erases the heterogeneities in surface mechanical properties. It has been previously shown that, for both

scanning strategies, the top surface microstructures of the repair consist of an alternation of small equiaxed grains and coarse columnar grains. Overall, the repairs show fine microstructures with a weak texture. The reader is invited to check the following article to learn more about the microstructural differences between the scanning strategies [18]. Furthermore, in this case, the same surface of the samples is loaded (the top surface). It has been shown in the literature that wear anisotropy can be observed depending on the tribologically stressed faces [8], [20], [21]. It is likely that in our case, if the lateral faces had been worn, we would have observed significant differences in wear volumes depending on the scanning strategy used. For the sake of clarity, the decrease in COF as well as wear volume with increasing temperature will be explained in the next section.

3.2. Impact of the normal load

The results obtained at elevated temperatures for different normal forces are compared to those obtained at room temperature. However, since the wear behavior at room temperature of this material deposited by LMD under these same tribological conditions has already been addressed in a previous publication [7], one can briefly summarize that the main wear mechanisms are primarily abrasion and adhesion. It is also worth noting that the microstructures of the repairs are greatly different from the IN718 conventionally manufactured. We especially observed that the conventional IN718 has a microstructure with less crystallographic default (i.e. a lower dislocation density) than the LMD IN718 repairs. Furthermore, due to the high cooling rates, detrimental phases for good wear resistance properties (such as Laves phases) are present in the microstructure of repairs. In contrast, these phases are not observed in the microstructure of conventionally formed IN718. More microstructural discrepancies were observed which encouraged this study (the reader is encouraged to read [7] for further information). However, in this study, we only study the wear behavior of the LMD repairs at high temperatures. A comparative study of the wear resistance of IN718 at high temperatures based on the forming process could be the subject of future research work.

As we demonstrated that the scanning strategy does not impact the wear behavior, the following results combine the data obtained for the two strategies studied. **Figure 4**a compares the average COF as a function of temperature and applied normal force. This highlights a decrease in the average COF with temperature. However, the normal force does not appear to significantly impact its average value. By examining the evolution of the COF for each of these conditions, as shown in **Figure 4**b and c, one can observe that, unlike tests at room temperature, at high temperatures, the COF stabilizes after a certain number of cycles. This COF stabilization is obvious for tests at 600°C. However, at 400°C, this stabilization is less pronounced or does not occur until the end of the test (especially for tests with a load of 50 N). The two tests repeated for each same tribological condition show how repeatable those results are. In order to better understand these COF evolutions, a characterization of the wear surfaces of the plane and the pin was conducted for each condition. These are presented in **Figure 5** and **Figure 6**.

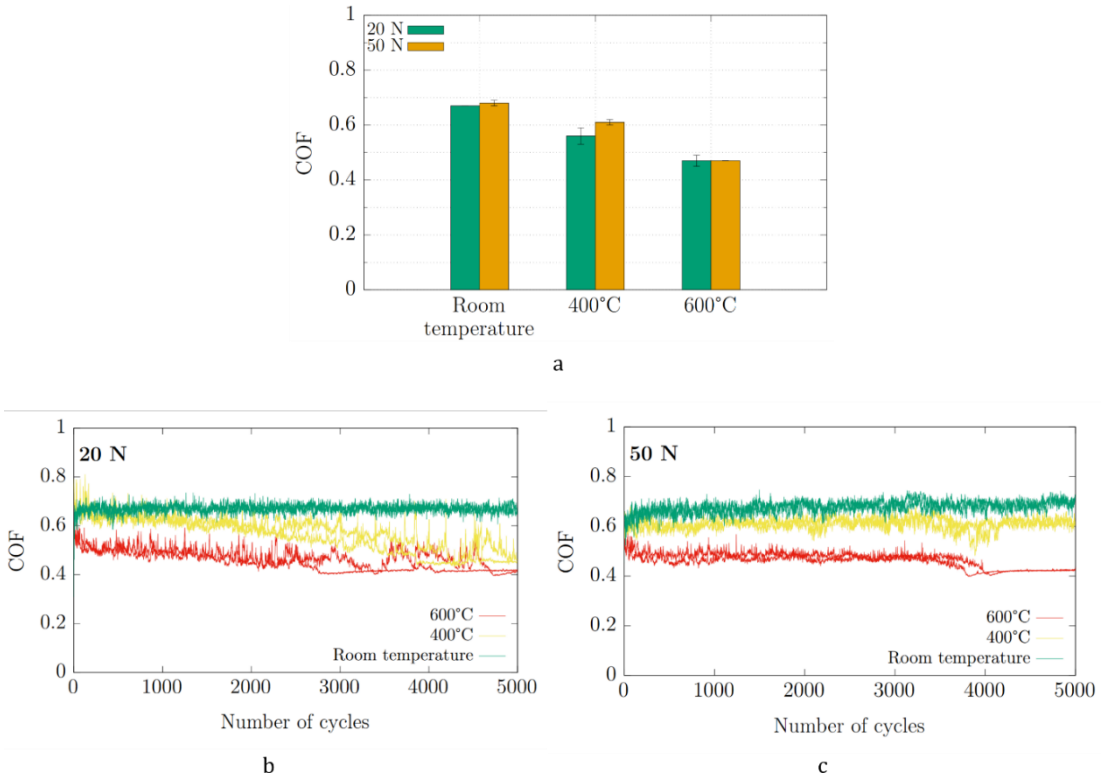

Figure 4. a) The average COF value as a function of temperature and normal force; Evolution of the COF as a function of the test temperature for a normal load of b) 20 N and c) 50 N.

The wear surface of the repair obtained for each of the studied tribological conditions are presented in **Figure 5**. At 20 N, the presence of oxide patches is observed. As indicated by the EDX points 1 and 3 in **Table 3**, these oxides are rich in nickel, chromium, and iron. Apart from these oxide patches, the oxygen content is much lower, demonstrating that these regions (points 2 and 4) correspond to the original IN718 with minimal oxidation. In these low-oxygen areas, wear grooves can be observed, indicating predominantly abrasive wear. At this normal force, the wear mechanisms on the plane are the same at both 400°C and 600°C. As shown in the BSE pictures, at 20 N the main wear mechanisms are abrasion and oxidation for both test temperatures.

At 50 N, differences in wear mechanisms are observed depending on the test temperature. At 400°C, no oxide patches are observed in the wear track. Instead, we observe on the BSE image grooves and adhered debris in the wear track which suggest abrasive and adhesive wear on the plane for this tribological condition. At 600°C, a significant amount of oxidized debris adhering to the surface is observed. The wear mechanisms under these loading conditions are similar to those observed at 20 N. Indeed, the BSE image shows oxidative and abrasive wear.

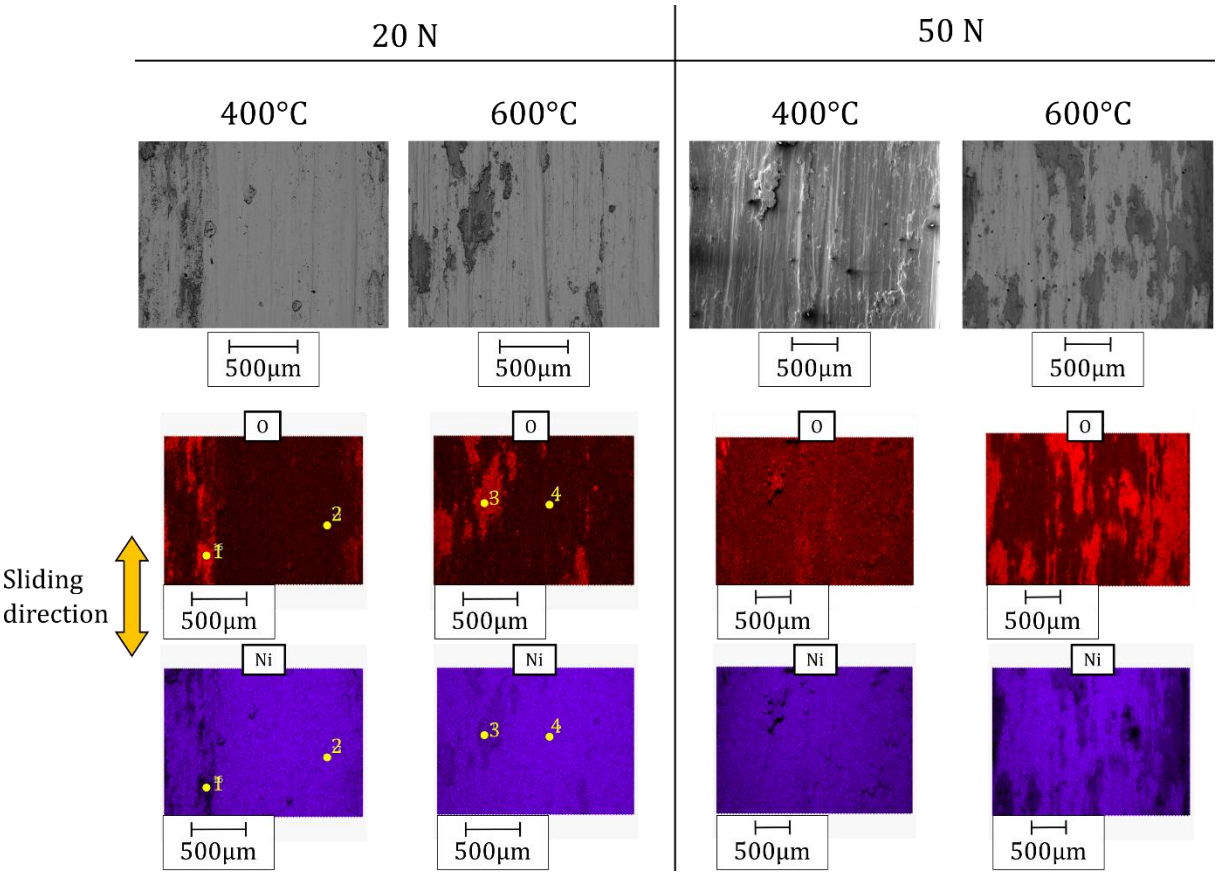

Figure 5. Backscatter electron (BSE) images and EDX maps taken in the wear tracks on the LMD IN718 plane for each tribological conditions.

Figure 6 compiles the wear features observed on the surface of the pin after wear. Firstly, it is obvious that for all the loading conditions, its surface is covered by IN718 debris. However, the oxidation of these adhered debris and their coverage vary depending on the test conditions. At 20 N and 400°C, it is observed that these debris are oxidized but do not completely cover the surface of the pin. Bands without oxidized debris aligned with the sliding direction are observed. In contrast, at 600°C, for both studied loads, the surface of the pin appears to be entirely covered by these highly oxidized debris. Finally, tribological tests at 400°C with a normal force of 50 N once again reveal wear mechanisms on the pin that are quite different from those observed previously. Indeed, under these tribological conditions, the surface of the pin is entirely covered by IN718 transfer layer. However, as indicated by EDX point 5 in **Table 3**, these debris are much less oxidized compared to the other tests.

Intuitively, it seems that the degree of pin coverage by oxidized debris is related to the final COF value after 5,000 cycles. To confirm this hypothesis, the final COF value was plotted as a function of oxide coverage on the surface of the pin in **Figure 7**. In this figure, only the tests at 20 N are plotted. It is also worth noting that the final COF value corresponds to the average value of the last 20 cycles of each test. **Figure 7** clearly demonstrates that, as the oxygen coverage rate increases, the COF decreases. This figure confirms that when the contact between the pin and the plane is separated by a homogeneous layer of adhered oxidized debris on the pin, the COF decreases. This third body, therefore, acts as a solid lubricant. The significant error bars at low percentage of coverage also demonstrate how unsteady the COF is when the pin is not well covered by those debris rich in oxygen.

Figure 7 confirms this hypothesis for the tests conducted at 20 N, but the same conclusion can be drawn for the tests at 50 N. Indeed, during the tests at 400°C, it was observed that the main wear mechanisms are abrasion and adhesion, leading to a high average COF (about 0.6). This can be explained by the fact that no oxidation phenomenon occurs, preventing contact lubrication. The COF is much higher because of the predominance of adhesion in those tribological conditions. The absence of oxidized debris in the contact can be explained by the fact that at this temperature, the oxide patches are not stable enough to withstand the significant shear stresses due to the high value of the load. Conversely, at 600°C, many adhered debris were observed on the surfaces of both contacting bodies because at this temperature, the oxidized debris persists in the contact despite the high shear stresses. The presence of these oxidized debris can explain the low average COF (about 0.47) in **Figure 4**a.

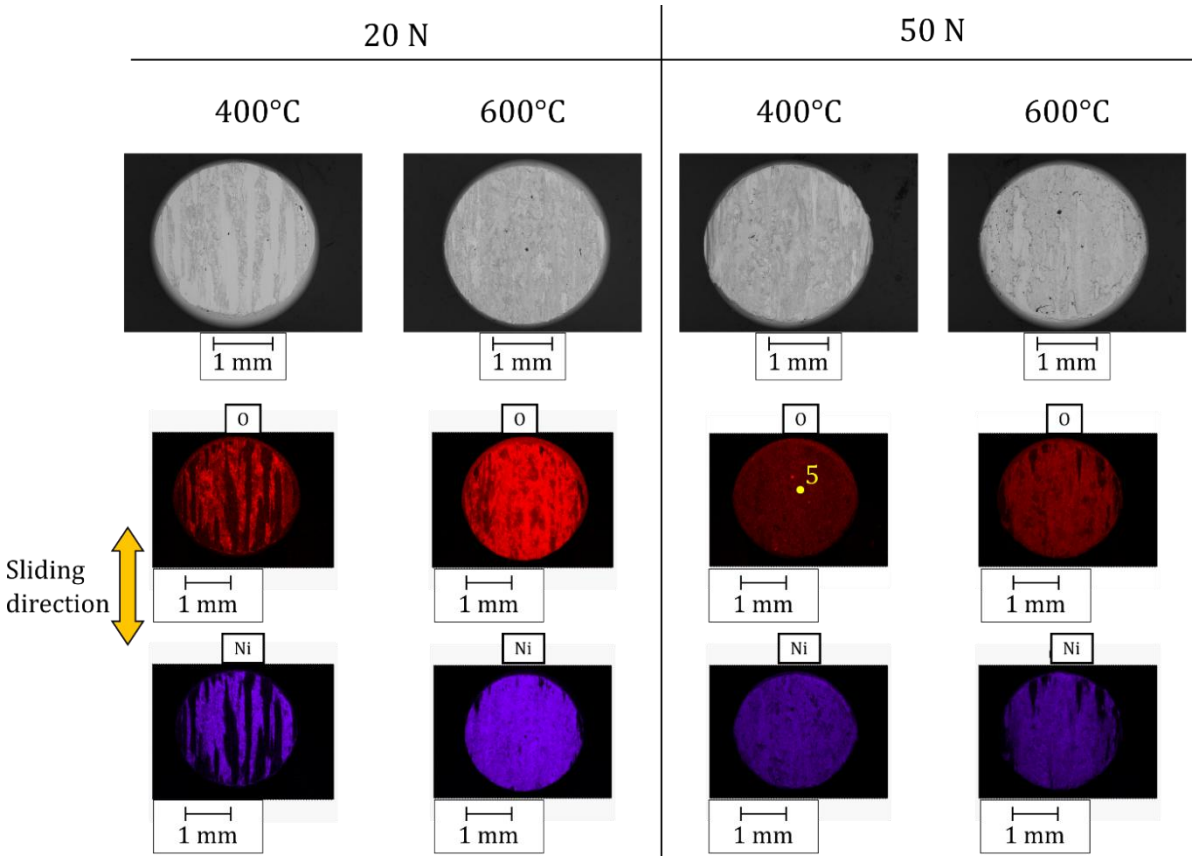

Figure 6. Backscatter electron (BSE) images and EDX maps of the contact surface of the pin for each tribological conditions.

Table 3 : Summary of the EDX points shown in **Figure 5** and **Figure 6**.

Element		O	Ni	Fe	Cr	Others
1	%w	22.2	18.0	41.5	7.2	11.1
	σ	0.2	0.5	0.4	0.1	-
2	%w	1.3	52.6	16.5	17.3	12.3
	σ	0.1	0.4	0.3	0.2	-
3	%w	20.0	41.7	17.4	10.5	10.4
	σ	0.4	0.9	0.6	1.8	-
4	%w	4.1	49.4	19.4	13.6	13.5
	σ	0.1	0.6	0.5	0.9	-
5	%w	2.4	48.4	24.0	14.6	10.6
	σ	0.1	0.7	0.6	0.3	-

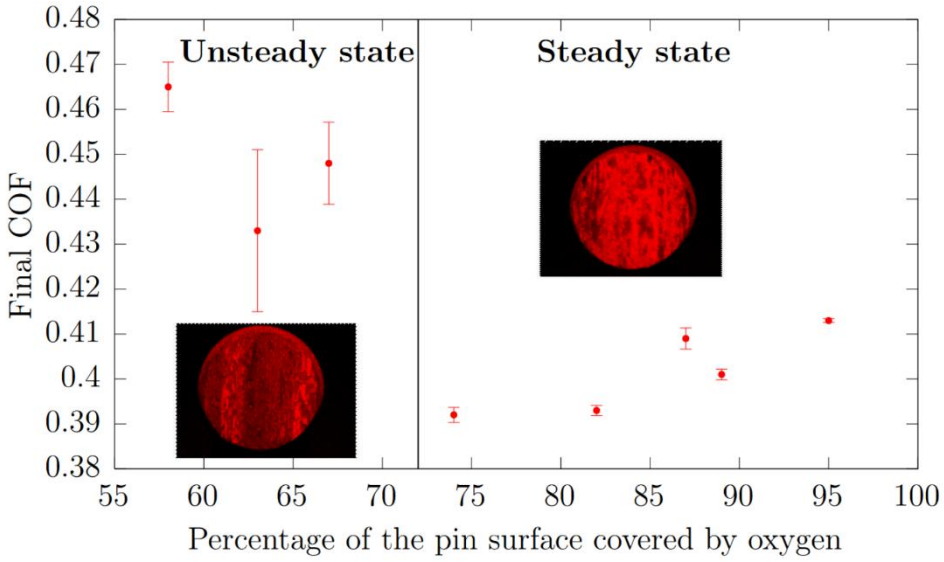

Figure 7. Final COF (average over the last 20 cycles) as a function of the percentage of coverage of the surface of the pin by oxygen (tests performed at 400°C and 600°C and with normal load of F_N = 20 N).

The quantification of wear on both surfaces is summarized in **Figure 8**. The wear volume of the repair as a function of temperature and normal force is shown in **Figure 8**a. The wear volume evolves differently depending on the normal force. At 20 N, the wear volume initially decreases as the temperature increases. This reduction in wear volume can be primarily explained by the appearance of the layer of adhered oxidized debris that lubricates the contact and protects the plane. It is noted that the difference in wear volume between tests at 400°C and 600°C is not significant, which can be attributed to the fact that the wear mechanisms are the same for these two tribological conditions. Through the study of the wear resistance of IN718 cold spray coatings, Sun et al. observed the emergence of oxides patches that also had the unique characteristic of reducing the coefficient of friction and wear rate [22]. They refer to the layer formed by these oxides as the glaze layer. It has been observed in numerous research that nickel-based alloys can form a glaze layer when subjected to tribological stresses at high temperature [13], [23]. Stott et al. explained the formation of such a layer through the compression and compaction of oxidized debris that form at the beginning of the wear process [24]. This glaze layer tends to become more stable as the temperature increases [25].

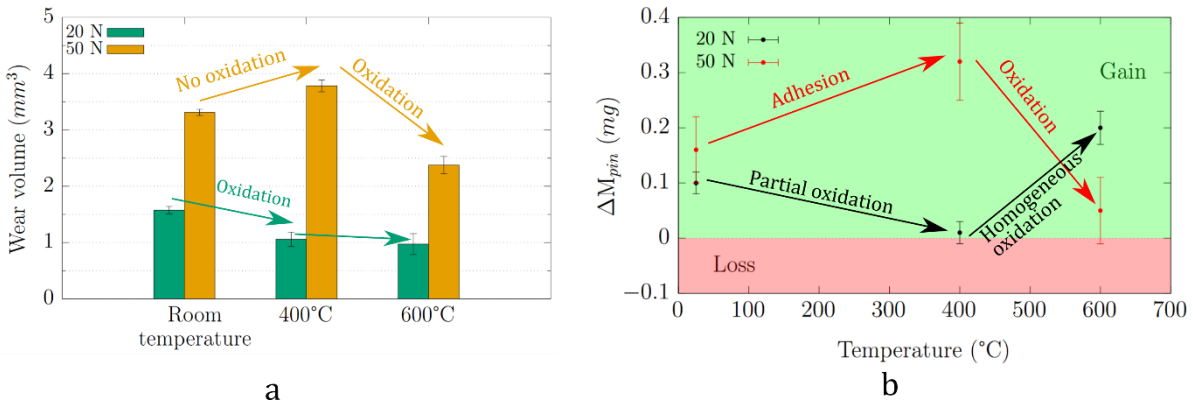

Figure 8. a) Wear volume of the LMD repair and b) evolution of the pin's mass as a function of the temperature and the normal load.

At 50 N, the wear volume initially increases as the temperature goes from room temperature to 400°C. This result can be explained by the fact that, as previously shown, no trace of the glaze layer was observed in the wear track and on the pin. Indeed, the wear mechanisms are the same as those observed at room temperature, namely adhesion and abrasion. The reason why the wear volume is greater than at room temperature is likely due to the decrease in the material's mechanical properties at this temperature. Then, at 600°C, the wear volume decreases dramatically to reach a value lower than that obtained at room temperature (approximately 2.4 mm^3). This trend can be explained by the appearance of an oxidized debris layer that lubricates the contact and limits the wear on the plane.

As shown in **Figure 8**b, the mass difference of the pin is always positive, which reflects a mass gain. From room temperature to 400°C, a decrease in the mass gain of the pin at 20 N is observed, which is likely due to the partial coverage of the pin's surface by compacted oxidized debris. In contrast, at 50 N, the mass gain of the pin increases due to the strong adhesion of slightly oxidized IN718 debris. At 600°C with a 20 N load, the mass gain is more significant than at 400°C, mainly because of the nearly complete coverage of the pin's surface by oxidized debris. Finally, at the same temperature with a normal force of 50 N, a minimal mass gain of the pin is observed. This limited mass gain at 600°C could be explained by the presence of a thinner and less dense layer of oxidized debris under these conditions compared to 400°C.

Figure 9 represents the wear volume for each high-temperature test with a normal force of 20 N as a function of dissipated energy. Interestingly, the distributions of wear volume as a function of dissipated energy for each test temperature follow a linear trend. This trend can be explained by assuming that the repair no longer wears when the glaze layer is present in the contact. This implies that the plane only wears through abrasion and adhesion (prior to the appearance of the oxidized debris layer). The linear evolution of wear volume as a function of dissipated energy is common when such wear mechanisms govern wear [7], [26]. **Figure 9** shows that the slope, i.e. the energetic wear rate (in mm^3/J), is higher at 600°C than at 400°C and room temperature. The room temperature and 400°C tests are scattered according approximately the same slope. However, the mean wear volume is higher at room temperature. The mean wear volume difference is explained by the appearance of the protective glaze layer at 400°C whereas the similar slope might be explained by the similar mechanical properties of the IN718. Then, from 400°C to 600°C, the mean wear volume is similar because of the same wear mechanisms involved at those temperature. However, the distribution of the wear volume at 600°C has a steeper slope than at 400°C and room temperature likely due to the decrease in mechanical properties of the IN718 deposited by LMD. Finally, on average the dissipated energy is lower as the test temperature increases. This result is in agreement with the trend of the COF as a function of temperature shown in **Figure 4**b. The higher the temperature, the lower the COF, the lower the dissipated energy.

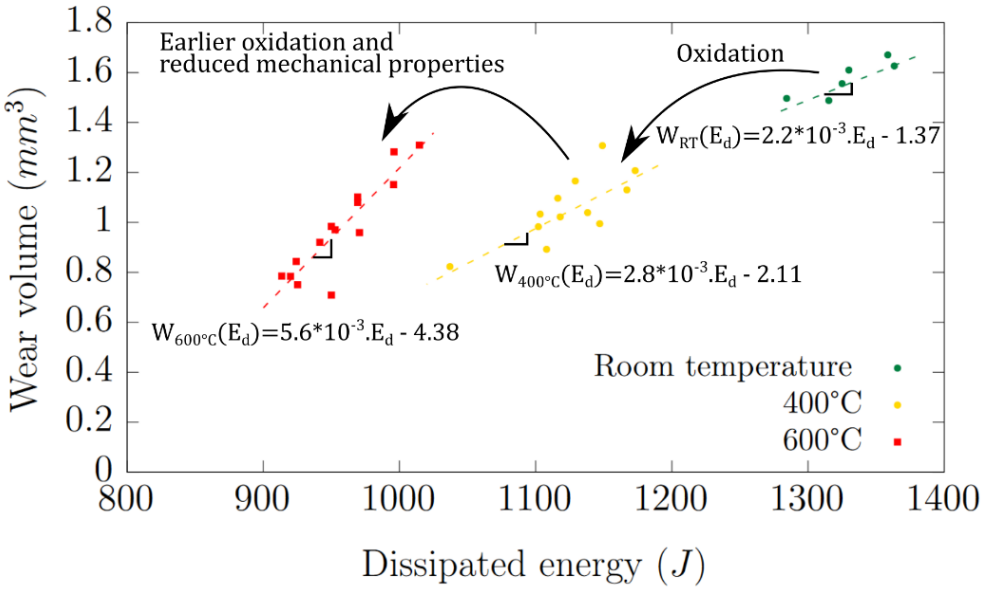

Figure 9. Wear volume as a function of the dissipated energy (results on both strategies are gathered in this graph).

Figure 10 summarizes all the observations made previously. In summary, for the two studied strategies, at 20 N, a glaze layer composed of compacted oxidized debris is formed partially (at 400°C) or completely (at 600°C) between the two bodies. During tests at 400°C with a normal force of 50 N, these oxidized debris do not adhere to the surface of the contacting bodies, resulting in abrasive and adhesive wear on the plane. Finally, at 600°C, glaze layer appears. Thus, when the glaze layer completely separates the two bodies, the latter lubricates and protects the plane from wear. Otherwise, severe wear driven by abrasion and adhesion occurs.

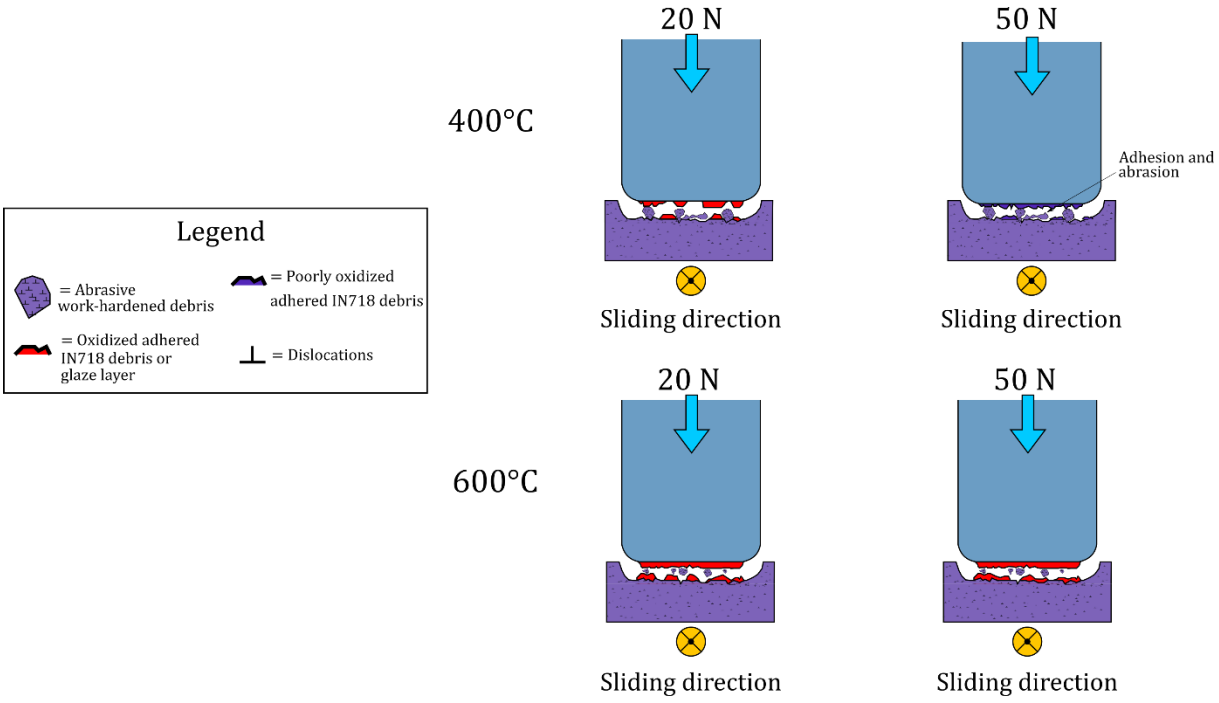

Figure 10. Schematics diagram summarizing wear mechanisms as a function of the applied normal force and temperature.

4. Conclusions

In this study, we investigated the tribological behavior of LMD-repaired IN718 as a function of laser scanning strategy, applied normal force, and temperature. The results demonstrated that the scanning strategy has no impact on the high-temperature wear behavior of LMD-repaired IN718. It is also shown that the homogeneity of the glaze layer in the contact plays a significant role in friction and wear. When this layer is evenly distributed in the contact, it acts as a solid lubricant and protects the plane from wear. As for the case of tests at 400°C with a high load, when mechanical stresses do not allow these debris to persist in the contact, the main wear mechanisms are abrasion and adhesion. These wear mechanisms lead to higher wear volumes than at room temperature. Finally, it was observed in the tests at low load that, despite very similar wear volumes, the wear rate of the LMD-deposited IN718 is higher at 600°C than at 400°C.

These results have provided a first insight into the high-temperature tribological behavior of LMD-repaired parts. Further research could be conducted to assess how these repairs perform in longer tests. Based on the previous results, one would expect to obtain higher wear volumes at 600°C than at 400°C if the glaze layer does not last. Additionally, it would be interesting to investigate how heat treatments affect the wear behavior of LMD-deposited IN718 and also to compare our tribological results with some performed on conventionally manufactured IN718.

Data Availability

The raw/processed data required to reproduce these findings cannot be shared at this time as the data also forms part of an ongoing study.

Competing of interest

The authors declare that they have no known competing financial interests or personal relationships that could have appeared to influence the work reported in this paper.

Acknowledgements

The authors want to thank the funders of this research: The Société nationale des chemins de fer français (SNCF, France) and the Direction Générale de l'Armement (DGA, France).

References

[1] R. Devine, C. Cullen, J. Foster, M. Kulakov, C. MacFadden, and S. Fitzpatrick, "Remanufacture of Hot Forging Dies By LMD-p Using a Cobalt Based Hard-Facing Alloy," *BHM Berg- und Hüttenmännische Monatshefte*, vol. 166, no. 5, pp. 243–249, 2021, doi: 10.1007/s00501-021-01108-z.

[2] Rahito, D. A. Wahab, and A. H. Azman, "Additive manufacturing for repair and restoration in remanufacturing: An overview from object design and systems perspectives," *Processes*, vol. 7, no. 11, 2019, doi: 10.3390/pr7110802.

[3] T. Ünal-Saewe, L. Gahn, J. Kittel, A. Gasser, and J. H. Schleifenbaum, "Process development for tip repair of complex shaped turbine blades with IN718," *Procedia Manuf.*, vol. 47, no. 2019, pp. 1050–1057, 2020, doi: 10.1016/j.promfg.2020.04.114.

[4] J. M. Wilson, C. Piya, Y. C. Shin, F. Zhao, and K. Ramani, “Remanufacturing of turbine blades by laser direct deposition with its energy and environmental impact analysis,” *J. Clean. Prod.*, vol. 80, pp. 170–178, 2014, doi: 10.1016/j.jclepro.2014.05.084.

[5] G. Bi and A. Gasser, “Restoration of nickel-base turbine blade knife-edges with controlled laser aided additive manufacturing,” *Phys. Procedia*, vol. 12, no. PART 1, pp. 402–409, 2011, doi: 10.1016/j.phpro.2011.03.051.

[6] B. G. Muralidharan, V. Shankar, and T. P. S. Gill, “Weldability of Inconel 718-A review,” 1996.

[7] T. Zurcher, G. Bouvard, J.-C. Abry, E. Charkaluk, and V. Fridrici, “Effect of the scanning strategy and tribological conditions on the wear resistance of IN718 obtained by Laser Metal Deposition,” *Wear*, vol. 534–535, p. 205152, 2023, doi: https://doi.org/10.1016/j.wear.2023.205152.

[8] F. Liu *et al.*, “The anisotropic wear and friction property of Inconel 718 superalloy fabricated by laser directed energy deposition,” *Tribol. Int.*, p. 108835, 2023, doi: https://doi.org/10.1016/j.triboint.2023.108835.

[9] Y. Xu, Y. Gong, P. Li, Y. Yang, and Y. Qi, “The effect of laser power on the microstructure and wear performance of IN718 superalloy fabricated by laser additive manufacturing,” *Int. J. Adv. Manuf. Technol.*, vol. 108, no. 7–8, pp. 2245–2254, 2020, doi: 10.1007/s00170-020-05172-6.

[10] B. Onuike and A. Bandyopadhyay, “Additive manufacturing in repair: Influence of processing parameters on properties of Inconel 718,” *Mater. Lett.*, vol. 252, pp. 256–259, 2019, doi: https://doi.org/10.1016/j.matlet.2019.05.114.

[11] X. Song, J. Lei, Z. Gu, and S. Zhou, “Boosting wear properties of Inconel718 superalloy by uniform dispersing graphene nanoplatelets through laser melting deposition,” *J. Alloys Compd.*, vol. 834, p. 155086, 2020, doi: 10.1016/j.jallcom.2020.155086.

[12] C. Hong *et al.*, “Laser metal deposition of TiC/Inconel 718 composites with tailored interfacial microstructures,” *Opt. Laser Technol.*, vol. 54, pp. 98–109, 2013, doi: 10.1016/j.optlastec.2013.05.011.

[13] Y. Liu *et al.*, “Tribological behaviors of LDED Inconel 718 samples polished with a hybrid laser polishing technique,” *J. Mater. Res. Technol.*, vol. 25, pp. 633–646, 2023, doi: 10.1016/j.jmrt.2023.05.230.

[14] S. Lu, J. Zhou, L. Wang, and J. Liang, “Effect of V and Cr transition layers on microstructure and mechanical properties of Ni-based coating on titanium alloy fabricated by laser cladding,” *Surf. Coatings Technol.*, vol. 405, no. December 2020, p. 126734, 2021, doi: 10.1016/j.surfcoat.2020.126734.

[15] C. Samuel. S, M. Arivarasu, and T. R. Prabhu, “High temperature dry sliding wear behaviour of laser powder bed fused Inconel 718,” *Addit. Manuf.*, vol. 34, no. April, p. 101279, 2020, doi: 10.1016/j.addma.2020.101279.

[16] Z. Xu *et al.*, “Study on the damage evolution of fretting wear in an Inconel 718 laser cladding alloy layer at different temperatures,” *Tribol. Int.*, vol. 179, no. November 2022, p. 108092, 2023, doi: 10.1016/j.triboint.2022.108092.

[17] A. Amanov, R. Karimbaev, C. Li, and M. Abdel, “Surface & Coatings Technology Effect of surface modification technology on mechanical properties and dry fretting wear behavior of Inconel 718 alloy fabricated by laser powder-based direct energy deposition,” *Surf. Coat.*

Technol., vol. 454, no. December 2022, p. 129175, 2023, doi: 10.1016/j.surfcoat.2022.129175.

[18] T. Zurcher, V. Fridrici, and E. Charkaluk, "Surface microstructure of an IN718 3D coating manufactured by Laser Metal Deposition," *Mater. Charact.*, p. 113054, 2023, doi: https://doi.org/10.1016/j.matchar.2023.113054.

[19] C. A. Schneider, W. S. Rasband, and K. W. Eliceiri, "NIH Image to ImageJ: 25 years of image analysis," *Nat. Methods*, vol. 9, no. 7, pp. 671–675, 2012, doi: 10.1038/nmeth.2089.

[20] M. Bahshwan, C. W. Myant, T. Reddyhoff, and M. S. Pham, "The role of microstructure on wear mechanisms and anisotropy of additively manufactured 316L stainless steel in dry sliding," *Mater. Des.*, vol. 196, p. 109076, 2020, doi: 10.1016/j.matdes.2020.109076.

[21] Y. Yang, Y. Zhu, M. M. Khonsari, and H. Yang, "Wear anisotropy of selective laser melted 316L stainless steel," *Wear*, vol. 428–429, no. January, pp. 376–386, 2019, doi: 10.1016/j.wear.2019.04.001.

[22] W. Sun *et al.*, "Tribological behavior of cold sprayed Inconel 718 coatings at room and elevated temperatures," *Surf. Coatings Technol.*, vol. 385, no. January, p. 125386, 2020, doi: 10.1016/j.surfcoat.2020.125386.

[23] L. Bai *et al.*, "Temperature-mediated tribological characteristics of 40CrNiMoA steel and Inconel 718 alloy during sliding against Si3N4 counterparts," *Friction*, vol. 9, no. 5, pp. 1175–1197, 2021, doi: 10.1007/s40544-020-0455-3.

[24] F. H. Stott and G. C. Wood, "The influence of oxides on the friction and wear of alloys," *Tribol. Int.*, vol. 11, no. 4, pp. 211–218, 1978, doi: https://doi.org/10.1016/0301-679X(78)90178-0.

[25] F. H. Stott, D. S. Lin, and G. C. Wood, "The structure and mechanism of formation of the 'glaze' oxide layers produced on nickel-based alloys during wear at high temperatures," *Corros. Sci.*, vol. 13, no. 6, pp. 449–469, 1973, doi: https://doi.org/10.1016/0010-938X(73)90030-9.

[26] J. F. Archard and W. Hirst, "The wear of metals under unlubricated conditions," *Proc. R. Soc. London. Ser. A. Math. Phys. Sci.*, vol. 236, no. 1206, pp. 397–410, Jan. 1956, doi: 10.1098/rspa.1956.0144.